Title

Osseointegration of Coarse and Fine Textured Implants Manufactured by Electron Beam Melting and Direct Metal Laser Sintering

Journal

3D Printing and Additive Manufacturing, 4(2)

ISSN

2329-7662

Authors

Ruppert, David S
Harrysson, Ola LA
Marcellin-Little, Denis J
et al.

Publication Date

2017-06-01

DOI

10.1089/3dp.2017.0008

Peer reviewed

3D PRINTING AND ADDITIVE MANUFACTURING
Volume 4, Number 2, 2017

DOI: 10.1089/3dp.2017.0008

ORIGINAL ARTICLE

Osseointegration of Coarse and Fine Textured Implants Manufactured by Electron Beam Melting and Direct Metal Laser Sintering

David S. Ruppert,[1] Ola L.A. Harrysson,[1,2] Denis J. Marcellin-Little,[1–3] Sam Abumoussa,[4] Laurence E. Dahners,[4] and Paul S. Weinhold[1,4]

Abstract

Osseointegrated implants transfer loads from native bone to a synthetic joint and can also function transdermally to provide a stable connection between the skeleton and the prostheses, eliminating many problems associated with socket prostheses. Additive manufacturing provides a cost-effective means to create patient-specific implants and allows for customized textures for integration with bone and other tissues. Our objective was to compare the osseointegration strength of two primary additive manufacturing methods of producing textured implants: electron beam melting (EBM) (mean Ra = 23 μm) and direct metal laser sintering (DMLS) (mean Ra = 10 μm). Due to spatial resolution, DMLS can produce surfaces with a roughness comparable to EBM. Two cohorts of Sprague-Dawley rats received bilateral, titanium implants in their distal femurs and were followed for 4 weeks. The first-cohort animals received EBM implants transcortically in one femur and a DMLS implant in the contralateral femur. The second cohort received DMLS implants (either fine textured or coarse textured to mimic EBM) in the intramedullary canal of each femur. Osseointegration was evaluated through mechanical testing and micro-computed tomography (bone volume fraction [BV/TV] and bone-implant contact [BIC]). The fixation strength of coarse textured implants provided superior interlocking relative to fine textured implants without affecting BV/TV or BIC in both cohorts. Coarse EBM implants in a transcortical model demonstrated an 85% increase in removal torque relative to the fine DMLS textured implants. The thrust load in the intramedullary model saw a 35% increase from fine to coarse DMLS implants.

Keywords: additive manufactured implants, electron beam melting, direct metal laser sintering, bone-implant interface, osseointegration of transcutaneous prostheses

Introduction

By 2050, the number of amputees in the United States is expected to double from ~1 in 190 in the year 2005.[1] Direct transcutaneous osseointegrated prostheses constitute an emerging alternative to traditional socket prostheses that offer a stable connection and the elimination of dermal lesions caused by the socket-skin interface. Osseointegrated implants also transfer loads from the residual native bone to a synthetic joint and back to the opposing bone in total joint replacements. In 2010, an estimated 4.7 million individuals living in the United States had a total knee implant and 2.5 million had a total hip implant.[2] The rates of new total knee and total hip arthroplasties in the United States are expected to increase to ~3.48 million and 572,000 per year, respectively, by 2030.[3] Additively manufactured (AM) implants provide a cost-effective means to customize the shape of the implant to interface with a patient's unique bone morphology

[1]Department of Biomedical Engineering, University of North Carolina-NC State University, Chapel Hill-Raleigh, North Carolina.
[2]Edward P. Fitts Department of Industrial and Systems Engineering, NC State University, Raleigh, North Carolina.
[3]Department of Clinical Sciences, College of Veterinary Medicine, NC State University, Raleigh, North Carolina.
[4]Department of Orthopaedics School of Medicine, University of North Carolina, Chapel Hill, North Carolina.

Opposite page: Additive manufactured implant designs for transcortical and intramedullary osseointegration to compare fine (*bottom center* and *right*) and coarse (*top center* and *left*) textures. *Photo credit:* Caroline Cross.

and allow for the customization of the surface texture that integrates directly with the bone and other tissues.

Electron beam melting (EBM) and direct metal laser sintering (DMLS) are the two primary methods for producing AM titanium implants for osseointegation. There have been several studies verifying the biocompatibility of titanium fabricated by these two methods.[4–6] However, there have been few studies comparing DMLS with EBM for osseointegration.[7] The objective of this study is to compare the osseointegration strength of two AM methods of producing textured implants: ''as-built'' coarse textured (mean ± standard deviation [SD]: Ra = 23 ± 2.9 μm) implants made by EBM and ''as-built'' fine textured (Ra = 10 ± 0.3 μm) and coarse textured (Ra = 23.1 ± 5.0 μm) implants made by DMLS.

Materials and Methods

Two *in vivo* studies were conducted with separate cohorts of animals. The first phase was developed to compare implants fabricated from two different additive manufacturing methods (EBM and DMLS) in a bilateral transcortical femoral metaphysis implant model. The transcortical model—similar to a dental implant—was used in the first phase to facilitate a second objective of developing and validating equipment for subsequent study. The second phase compared the fine surface texture of the DMLS implants with DMLS implants fabricated with a surface texture similar to that of an EBM implant. An intramedullary femur implantation model was utilized to better represent percutaneous osseointegrated implant and arthroplasty implant models as well as to develop a restraint system for administering therapies in a subsequent study.

Phase 1 animals

Animal work was approved by the University of North Carolina at the Chapel Hill Institutional Animal Care and Use Committee. Female retired breeder Sprague-Dawley rats (Charles River Laboratories, Wilmington, MA) with a mean age of 24 weeks were used. Rats were caged in pairs and given *ad libitum* access to food and water with a 12-h light/dark cycle (7 am to 7 pm) throughout the study.

Based on previous intramedullary implantation studies done with rats in the literature[8] and our own experience with a transverse implantation model in the rat tibia, we estimated an SD of 20% of the mean torque-out strength for the electron beam melted implants. To detect a 35% difference in strength between the two manufacturing methods with a power of 0.80 and an alpha of 0.05, a power analysis calculated that an N of 6 rats was required.

Implants

All implants were fabricated by using grade 5 Titanium (Ti-6Al-4V) and produced at a length of 7 mm and a diameter of 2 mm. A 1.39 mm flat-to-flat hex was machined on the last 2.86 mm of the EBM implants for insertion and torque-out testing, whereas the hex was additively fabricated on the DMLS implants due to superior spatial resolution (Fig. 1). EBM implants were produced on an Arcam A2 (Arcam, Mölndal, Sweden) by using a powder diameter ranging from 45 to 105 μm. The DMLS implants were manufactured on an EOS M290 (EOS GmbH, Krailling, Germany) by using a powder diameter of 25–45 μm.

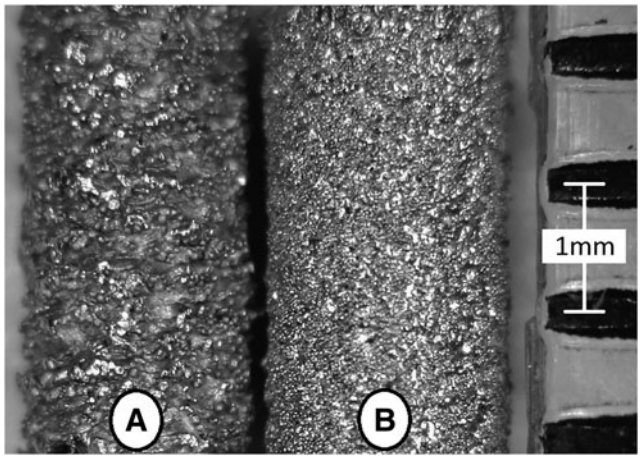

FIG. 1. EBM **(A)** versus DMLS **(B)** implant. DMLS, direct metal laser sintering; EBM, electron beam melting.

Implants were ultrasonically cleaned in a 1% Alconox 10 gm/L solution at 65°C for 15 min. The implants were rinsed twice with 65°C deionized water for 10 min under ultrasonic agitation. All implants were textured by acid etching in a 48% sulfuric acid (H_2SO_4) bath at 60°C and were agitated with a stir bar for 30 min.[9] The implants were rinsed in deionized water, dehydrated in a 70% ethanol solution, and allowed to air dry before packaging for sterilization by autoclave. The surface topography of both implants types was optically evaluated by using a Hirox KH-7700 microscope (Hirox-USA, Inc., River Edge, NJ), and the surface roughness (Ra) was obtained through a linear regression of the resulting spatial map.

Surgical model

Under isoflurane anesthesia, implants were surgically placed bilaterally in the medial cortex of the distal metaphysis of the femur through a lateral skin incision. Each animal received an EBM implant in a randomly selected femur and a DMLS implant in the contralateral limb. An 18-gauge needle (1.16-mm-diameter) was used to start the hole, whereas the final hole was drilled to 1.9 mm under saline irrigation. The incisions were closed by using wound clips (Autoclips; MikRon Precision, Gardena, CA) and tissue adhesive (TA5; Med Vet International, Mettawa, IL). The clips were removed 12 days after the surgery when radiographs were made. All animals were given a 0.8 mg/kg injection of sustained-release buprenorphine and were given *ad libitum* access to acetaminophen-doped drinking water (1.6 mg/mL) for 7 days after surgery.

The rats' masses were recorded on arrival, immediately before surgery, and after euthanasia. The rats were followed for 4 weeks after surgical placement of implants. The animals were humanely euthanatized 4 weeks after surgery. Femurs were collected, wrapped in saline-soaked gauze, and stored at −20°C until testing.

Radiographs

Radiographs were made by using a cabinet radiographic unit (HP 43804 X-Ray System Faxitron; Hewlett Packard, Palo Alto, CA) at 12 days after surgery by using dental X-ray film (DX-42; Henry Schein, Melville, NY) at 35 kV with a 12-s aperture exposure. Radiographs were used to

confirm the implant location and to verify the absence of femoral fractures.

Ex vivo *micro-computed tomography*

All femur pairs were scanned by using a micro-computed tomography (μCT) (40 model specimen CT; Scanco Medical, Brüttisellen, Switzerland) with a 16 mm field of view on medium resolution with a voxel size of 16 μm. The X-ray power setting was 70 kVp, 114 μA, and 8 W. The scans had an integration time of 300 ms and were averaged once. Specimens were soaked in a 1:100 dilution of protease inhibitor cocktail (Sigma-Aldrich #P8340, St. Louis, MO) with saline before μCT.

The resulting μCT scans were analyzed by using software developed for processing medical images (Mimics 16.0; Materialise, Plymouth, MI), as shown in Figure 2. The implant was dilated by five pixels (80 μm) to exclude the metal-induced artifact as determined by a prior study.[10] The bone was segmented out by using a low and high threshold of 529 and 1615 mgHA/cm^3, respectively. The implants were segmented by using a threshold ≥2249 mgHA/cm^3. The total area of the implant was obtained and divided by its length. This area per unit length was used later for normalizing the torque results.

The bone volume fraction (BV/TV) within 500 μm of the implant was calculated.[11] A cylinder was constructed in the femur that had a diameter of 1000 μm, which was larger than the mean diameter of the implant. The volume of bone within this region was divided by the volume of the cylinder minus the dilated implant volume within the cylinder. The resulting percentage represented the medullary BV/TV.

The bone-implant contact (BIC) was calculated along the length of the implant embedded in the femur. The percent BIC was determined as the ratio of voxel threshold as bone to the total number of voxel adjacent to the dilated implant.

Mechanical testing

After the μCT evaluation, the mechanical stability of osseointegration of the implants was evaluated through torsional removal. A polymer resin (number 265; 3M Bondo, Atlanta, GA) in conjunction with a tapered mold was used to pot the specimens in the proper orientation to interface with a material testing system (MTS) (8500 Plus; Instron, Norwood, MA). A chain and sprocket on a custom fixture were used to transfer the rotary motion of implant removal to the uniaxial servohydraulic motion of the MTS. The angular rotation and torque were measured by using a potentiometer (Series P2201; Novotechnik US, Southborough, MA) and a 350 N·mm torque cell (Model 2105-50; Honeywell Sensotec, Columbus, OH), respectively. A Jacob's chuck that attached to the torque cell and then slid along a linear slide was utilized to transmit torque to the hexagonal head of the implant while minimizing translational loads to the femur in the tapered mold. A prior study has shown the maximum torque and stiffness to be independent of angular velocity in the range of 3–12°/s angular velocity.[12] Thus, specimens were preloaded with 3 N·m and torqued at a constant rate of 6°/s until failure of the bone-implant interface was reached.

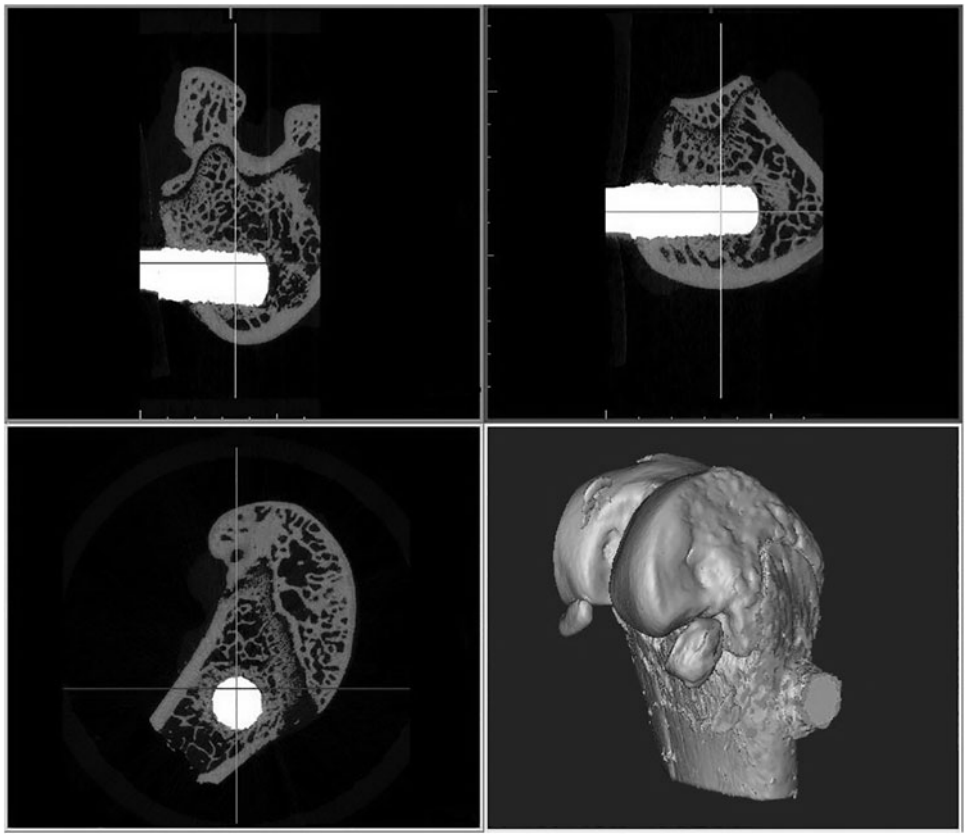

FIG. 2. Typical *ex vivo* micro-computed tomography scan of phase one specimens viewed in Mimics.

Maximum torque and stiffness were determined from the resulting torque and rotational displacement data by using a program developed in Labview (Labview 6.0; National Instruments, Austin, TX). Stiffness was determined by the slope of the regression line of the torque–deflection angle curve between limits of 25% and 75% of the maximum torque.[13] The maximum torque was normalized to calculate the equivalent shear stress at the bone-implant interface by dividing the resulting value by the product of the implant's surface area in the femur and the mean radius of the implant, both of which are obtained from the μCT analysis.

Statistical analysis

A one-way repeated-measures analysis of variance (implant type) with Holm-Sidak *post hoc* mean comparison testing for all outcome measures was performed on the results by using a statistical analysis program (SigmaPlot v11.0; Systat Software, San Jose, CA).

Phase 2 animals

The animal model for the second phase was identical to that of the first phase. However, rats were caged in groups of three, based on allowable housing density for rat weight. Based on a power analysis, 10 rats were used in the second cohort of animals.

Implants

Implants were fabricated by using Grade 5 Titanium (Ti-6Al-4V). The titanium rods were produced at lengths of 20 mm and diameters of 1.5 mm with a 1.6 mm boss on the last 1.5 mm and a dimple in each end to facilitate surgical implantation and mechanical pushout. The implants were built by using DMLS on an EOS M280 15° from vertical with a beam offset of 0.09 mm and a powder size ranging from 25 to 45 μm. Two different groups of implants were built: one with the fine native surface texture and one with a surface texture designed to simulate the Ra value of the coarse native EBM surface texture. The surface topographies of the DMLS implants were optically evaluated, and surface roughness (Ra) was calculated as in the first phase (Fig. 3). The implants were cleaned, etched, and sterilized as in the first phase.

Surgical model

The surgical model was changed from the trans-femoral model of the first phase to an intramedullary model. Following the same pre- and post-surgical methods as earlier, implants were surgically placed bilaterally in the intramedullary canal of the distal femur through a craniolateral skin incision. The right limb randomly received either a fine or a coarse textured DMLS implant whereas the contralateral limb received the alternative implant texture. After subluxation of the patella, an 18-gauge needle (1.16 mm-diameter) was used to start a hole in the intracondylar notch whereas the final hole was reamed and extended to a 21 mm depth manually with a 1.5 mm twist bit. The DMLS implant was inserted by manual thrust and torque into the drilled hole until it was flush with the articular surface. The patella was returned to its original position, and the knee joint was closed with an absorbable suture. Skin incisions were closed as in the first phase. The animals were followed for 4 weeks.

Animal care, radiographs, euthanasia, and specimen collection and storage were performed as in the first phase. The statistical analyses used to compare the results of the second phase were identical to the first phase.

Ex vivo *μCT*

Osseointegration was evaluated by BV/TV and BIC along a 2.5 mm length, 2 mm from the proximal end and along a 6 mm length 1.5 mm from the distal end of the implant by

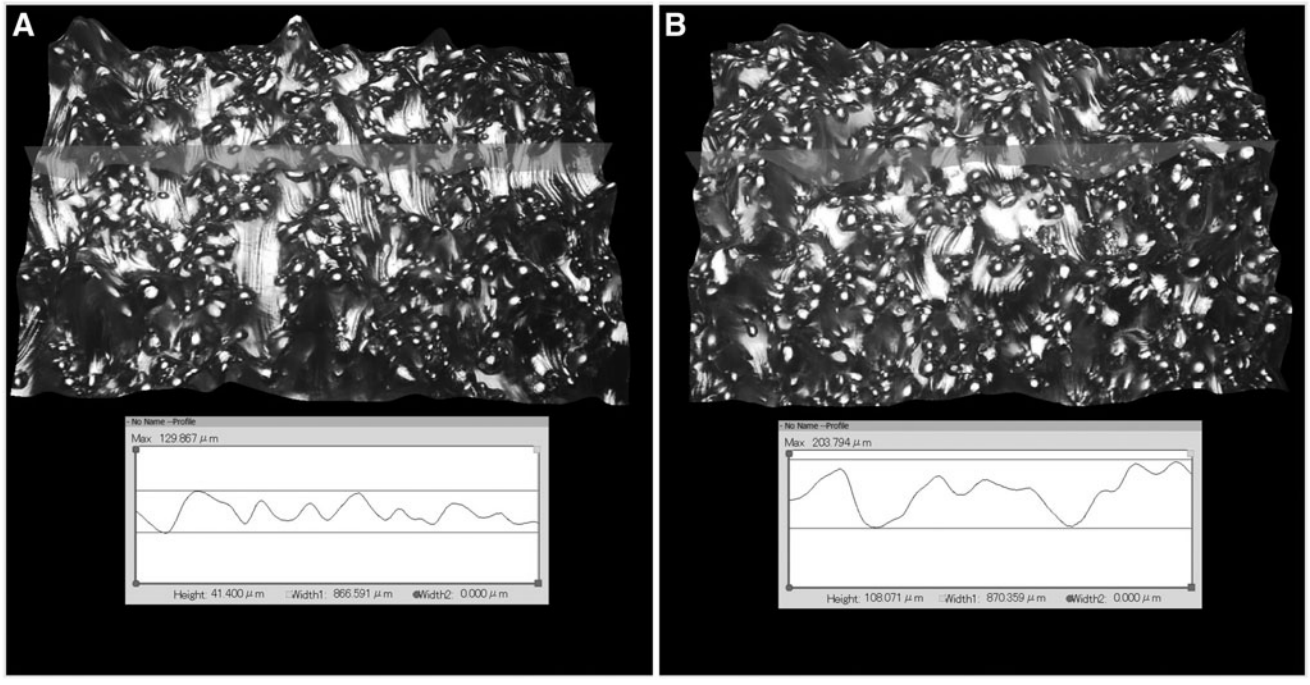

FIG. 3. **(A)** surface topography of fine textured DMLS implant, **(B)** surface topography of coarse textured DMLS implant.

using μCT (Fig. 4). All of the femur pairs of the second phase were processed by using the same method as the first phase. However, a 10 mm field of view on medium resolution with a voxel size of 12 μm was utilized due to the implant running along the longitudinal axis of the femur. The dilation of the implant to five pixels results in a distance of 60 μm due to the reduction in voxel size. This decreased region still agrees with the prior study.[10] The region of BV/TV surrounding the implant was reduced to 250 μm to decrease deviation induced by the implants' random proximity to the cortical shell.

Mechanical testing

After the μCT evaluation, pushout testing on all specimens was performed to assess osseointegration by evaluating the stiffness and the allowable shear of the bone-implant interface. Before mechanical testing, the proximal ends of the femurs were removed by using a fine-toothed rotary bone saw to allow pushout of the implants. Specimens were potted in a custom-tapered mold by using a self-curing acrylic resin (Ortho Jet BCA, Lang Dental, Wheeling, IL) and allowed to cure for 30 min. The axis of the implant was aligned in the direction of pushout with two opposing tapered pins, which rested in the dimple at each end of the implant while the resin set. A 3 mm diameter, 2 mm thick silicone disk was used during potting to ensure consistent support of the femoral condyles during mechanical testing while allowing an opening for the implant to be pressed through. The specimens were kept hydrated by submerging the potting fixture into a beaker with 250 mL of 27°C saline while the resin cured for 20 min followed by wrapping the specimen in saline-soaked gauze for the remaining 10 min.

Mechanical testing was carried out with an MTS (8500 Plus; Instron Corp.). The uniaxial servohydraulic motion of the MTS was transferred to the implant through a tapered stainless steel pin secured in a Jacob's chuck (Fig. 5). Linear load was measured with a 500 N load cell. The potted specimen was allowed to sit squarely on a platform with a hole in the center for implant pushout. Specimens were preloaded with 5 N and pushed out at a constant rate of 2 mm/min until failure of the bone-implant interface was reached. Maximum load and stiffness were determined from the resulting data by using the system software. The maximum load was normalized by dividing the maximum axial load by the implant's surface area obtained from the μCT analysis. This normalization was done to calculate the equivalent shear stress at the bone-implant interface.

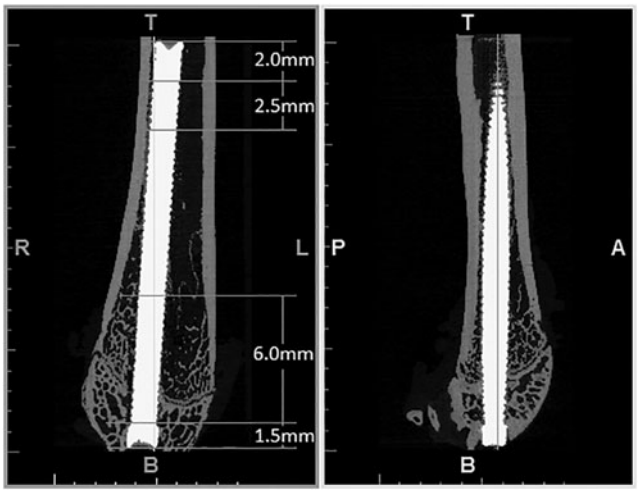

FIG. 4. Distal femur with intramedullary implant.

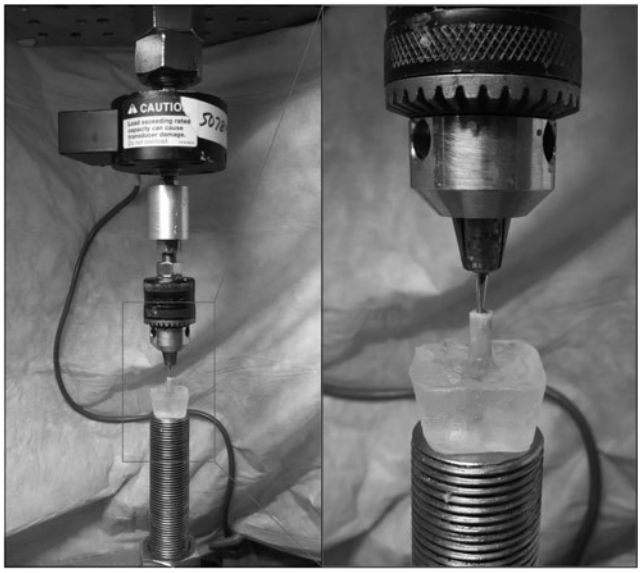

FIG. 5. Mechanical pushout fixture with potted specimen.

Results

Animals in the first cohort had a mean ± SD weight of 342 ± 25 g at surgery. The mean weight loss between surgery and euthanasia was 12 g. The second cohort had a mean group weight of 341 ± 25 g at surgery. Rats lost a mean body weight of 3 g per animal between surgery and euthanasia.

Implant location and bone response for both phases of the study were assessed by using radiographs. Femoral fractures were not seen in either phase of the study. Therefore, all limb pairs of the first phase and six matched pairs from randomly selected animals of the second phase underwent μCT. Mechanical stability analysis was also conducted on all limb pairs for both phases.

The finished implants for the first phase had mean ± SD major diameters of 1.86 ± 0.00 mm and 1.91 ± 0.03 mm for the EBM and DMLS implants, respectively. The area per length determined through μCT was 9.23 ± 0.25 mm^2/mm for EBM implants and 8.13 ± 0.12 mm^2/mm for DMLS implants. The intramedullary implants for the second phase all had the same diameter of 1.50 ± 0.00 mm and had an average area per length of 5.57 ± 0.09 mm^2/mm and 5.75 ± 0.04 mm^2/mm for fine and coarse implants, respectively. The surface topography analysis revealed that EBM-produced implants had a mean ± SD ''as-built'' surface roughness of Ra = 23 ± 2.9 μm. Conversely, DMLS generated implants had a mean ''as-built'' surface roughness of Ra = 10 ± 0.3 μm. The DMLS process for the second phase of the study produced a surface roughness of Ra = 7.7 ± 1.8 μm and Ra = 23.1 ± 5.0 μm for fine and coarse implants, respectively.

In phase 1, maximum removal torque (+85%, $p = 0.003$) and energy to failure (+109%, $p = 0.019$) were higher in EBM than fine textured DMLS implants (Fig. 6). In phase 2, the maximum thrust load (+35%, $p = 0.007$) and energy to failure

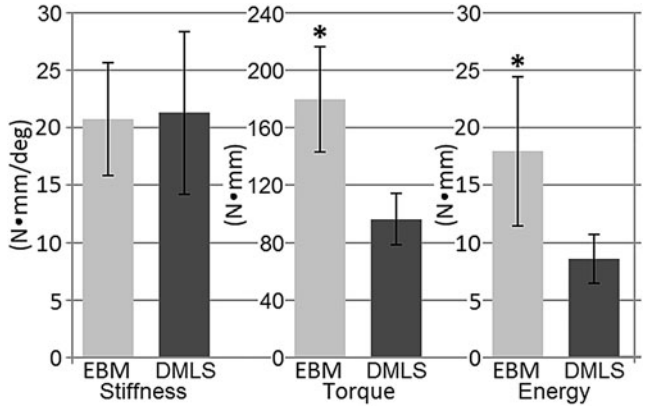

FIG. 6. Mechanical torque-out results of phase 1 specimens. *denotes significant difference ($P < 0.05$).

(+41%, $p = 0.019$) were larger for coarse textured DMLS implants than fine textured DMLS implants (Fig. 7). Bone-implant stiffness, BV/TV, and BIC did not differ for various implant types for both phases of the study (Table 1). Phase 2 results developed a statistically significant correlation between the max load and stiffness ($r = 0.7228$, $p < 0.001$). However, the results of phase 1 did not establish a statistically significant correlation ($r = -0.1083$, $p = 0.78$).

The removal loads of both the first and second phase were normalized as equivalent shear-forces to better compare the results between the torsional testing of the transcortical implants and the pushout of the intramedullary implants. In phase 1, the equivalent shear-force was larger (+59%, $p = 0.003$) for EBM implants than fine textured DMLS implants. The mean equivalent shear-force of the coarse textured DMLS implants of phase 2 showed a +27% increase relative to the fine textured DMLS implants but did not differ statistically (Fig. 8).

In the first phase, difficulties were encountered with surgical placement for two specimens and another specimen was overloaded at dissection. Due to the complications, these three specimens were excluded from implant comparisons.

Discussion

The coarse textured surface of the EBM design yielded higher torsional properties compared with the fine textured DMLS design, highlighting the increased interlocking area between the bone and implant for a given implant diameter. Due to the DMLS' superior spatial resolution, it is possible to manufacture an implant by DMLS with a similar surface roughness as the EBM implants while allowing for a more detailed geometry. Phase 2 of this study examined the osseointegration of such coarse DMLS implants. The fixation strength of coarse DMLS implants was also proven to provide superior interlocking relative to the fine textured DMLS implants. Such a statistically significant difference in torsional strength between coarse textured implants and fine textured implants is supported by a similar work by Wennerberg *et al.*, where a similar phenomenon was seen when comparing various sand-blasted titanium screw implants.[14] Interestingly, implant roughness in both phases of this study did not affect the BV/TV or the BIC. This finding supports previous observations that BIC is unrelated to surface roughness.[15]

It was demonstrated in this study that maximum pushout load correlated to the bone-implant stiffness. However, fixation strength in phase 1 exhibited low variation within the implant types and, thus, failed to draw a correlation between removal torque and implant stiffness, converse to the results of phase 2.

Table 1. Mean ± Standard Deviation Bone Volume Fraction (Measured Within 500 μm of Implants for Phase 1 and 250 μm Excluding Cortical Regions of Implants for Phase 2 Scans) and Bone-Implant Contact Relative to Available Area of Embedded Implant

Implant type	*BV/TV*	*BIC*
Phase 1, %		
Fine	70.3 ± 3.8	73.5 ± 9.0
Coarse	74.9 ± 2.7	80.4 ± 7.0
Phase 2—Distal, %		
Fine	28.4 ± 7.4	36.5 ± 5.2
Coarse	30.6 ± 7.2	37.6 ± 4.7
Phase 2—Proximal, %		
Fine	5.6 ± 3.5	14.4 ± 7.9
Coarse	6.1 ± 5.4	15.9 ± 8.3

Groups did not differ statistically.
BIC, bone-implant contact; BV/TV, bone volume fraction.

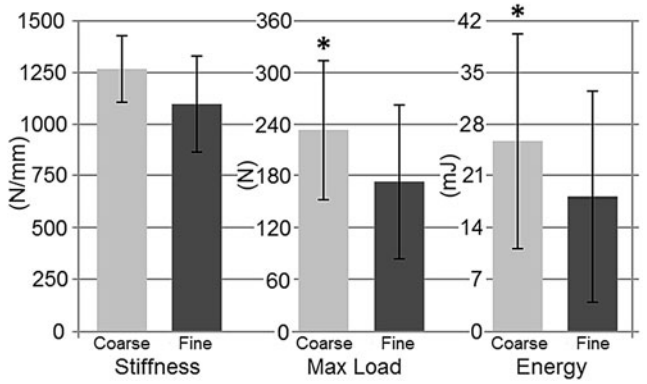

FIG. 7. Mechanical pushout results of phase 2 specimens. *denotes significant difference ($P < 0.05$).

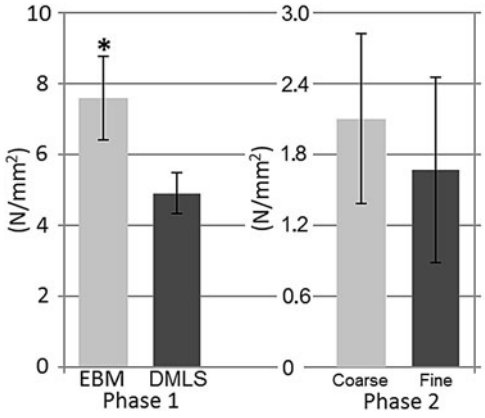

FIG. 8. Maximum equivalent shear-force of implants as a function of implant area. *denotes significant difference ($P = 0.003$).

Placing the implants in the intramedullary canal resulted in more variability in cortical contact proximally and, subsequently, larger variations in equivalent shear-force. It was also noted that the equivalent shear-force for phase 2 was considerably lower than that for phase 1. This is most likely due to decreased implant contact with the cortical shell for the available surface area. Cortical bone may provide superior mechanical stability in osseointegrated implants compared with trabecular bone. Matching the implant to the residual bone would greatly increase the contact with the cortical shell and, therefore, should also enhance mechanical stability of osseointegration, highlighting the potential benefits of patient-specific implants.

This study was not without limitations. Histological analysis results in a planar image of the BIC interface, however, excluding information around the remainder of the implant perimeter. μCT evaluation allows for a non-destructive analysis of the BIC interface around the entire implant perimeter. This study's μCT evaluations were performed with an offset implant surface to exclude the metal-induced artifact determined in a prior study.[10] The exclusion of information immediately adjacent to the implant may reduce the sensitivity to detect meaningful differences in BIC.

Conclusion

As the trend in amputee prosthetic devices moves toward transcutaneous osseointegrated implants instead of socket-cup fitting prosthetic devices, this study is important in showing that additive manufacturing can provide a means of producing well-fitted osseointegrated implants that can be easily customized. AM implants provide a means to produce customized geometries to match patient-specific anatomy as well as customized surface textures for optimizing implant stability. This research indicates that coarse textured surfaces can provide a higher interface strength for titanium alloy implants than fine textured surfaces. Future studies should be conducted to determine the optimal roughness for implant fixation. Another question left unanswered is whether there is an optimum surface roughness interaction between cortical bone and an implant compared with trabecular bone and an implant.

Acknowledgments

This work was supported by the National Science Foundation under Award Number CBET-1441636. Any opinions, findings, and conclusions or recommendations expressed in this material are those of the authors and do not necessarily reflect the views of the National Science Foundation. The authors thank the Small Animal Imaging Facility at the UNC Biomedical Imaging Research Center for providing the μCT imaging service, and the imaging core is supported, in part, by an NCI cancer core grant, P30-CA016086-40. They also thank Melanie Card for her technical assistance with the analysis of μCT DICOM stacks. Gratitude also goes to EOS North America for fabricating the DMLS implants on short notice for the first phase of the study.

Author Disclosure Statement

No competing financial interests exist.

References

1. Ziegler-Graham K, MacKenzie EJ, Ephraim PL, *et al.* Estimating the prevalence of limb loss in the United States: 2005 to 2050. Arch Phys Med Rehabil 2008;89:422–429.
2. Kremers HM, Larson DR, Crowson CS, *et al.* Prevalence of total hip and knee replacement in the United States. J Bone Joint Surg Am 2015;97:1386–1397.
3. Kurtz S, Ong K, Lau E, Mowat F, *et al.* Projections of primary and revision hip and knee arthroplasty in the United States from 2005 to 2030. J Bone Joint Surg Am 2007;89:780–785.
4. Wang H, Zhao B, Liu C, Wang C, Tan X, Hu M. A comparison of biocompatibility of a titanium alloy fabricated by electron beam melting and selective laser melting. PLoS One 2016;11:e0158513.
5. Hoa YL, Li SJ, Yang R. Biomedical titanium alloys and their additive manufacturing. Rare Metals 2016;35:661–671.
6. Sidambe AT. Biocompatibility of advanced manufactured titanium implants—a review. Materials 2014;7:8168–8188.
7. Biemond JE, Hannink G, Verdonschot NJJ, Buma P. Bone ingrowth potential of electron beam and selective laser melting produced trabecular-like implant surfaces with and without a biomimetic coating. J Mater Science 2013;24: 745–753.
8. Chen B, Li Y, Xie D, *et al.* Low-magnitude high-frequency loading via whole body vibration enhances bone-implant osseointegration in ovariectomized rats. J Orthop Res 2012; 30:733–739.
9. Ban S, Iwaya Y, Kono H, *et al.* Surface modification of titanium by etching in concentrated sulfuric acid. Dent Mater 2006;22:1115–1120.
10. Liu S, Broucek J, Virdi AS, *et al.* Limitations of using micro-computed tomography to predict bone-implant contact and mechanical fixation. J Microsc 2012;245: 34–42.
11. Ogawa T, Zhang X, Naert I, *et al.* The effect of whole-body vibration on peri-implant bone healing in rats. Clin Oral Implants 2010;22:302–307.
12. Lepola V, Vaananen K, Jalovaara P. The effects of immobilization on the torsional strength of the rat tibia. Clin Orthop Relat Res 1993;297:55–61.
13. Miles J, Weinhold P, Brimmo B, *et al.* Rat tibial osteotomy model providing a range of normal to impaired healing. J Orthop Res 2011;29:109–115.
14. Wennerberg A, Albrektsson T, Andersson B. Bone tissue response to commercially pure titanium implants blasted with fine and coarse particles of aluminum oxide. Int J Oral Maxillofac Implants 1996;11:38–45.
15. Wennerberg A, Albrektsson T, Andersson B, *et al.* A histomorphometric and removal torqued study of screw-shaped titanium implants with three different surface topographies. Clin Oral Implants Res 1995;6:24–30.

Address correspondence to:
David S. Ruppert
University of North Carolina
Orthopaedic Research Labs
134 Glaxo Building, CB# 7546
101A Mason Farm Road
Chapel Hill, NC 27599

E-mail: dsrupper@ncsu.edu